Magnetic-Thermal Coupling Analysis of Air-Core Reactor in EAST Fast Control Power Supply

Hu Yunpeng[1] *Bao Xiaohua*[1] *Zhang Cheng*[1] *Chen Yuanyang*[1] *Gao Ge*[2]

(1. School of Electrical Engineering and Automation Hefei University of Technology Hefei 23009 China
2. Chinese Academy of Sciences Institute of Plasma Physics Hefei 23000 China)

Hu Yunpeng (胡云鹏), male, was born in 1992, a postgraduate. his main research interests are in the field of magnetic field analysis and electromagnetic shielding.

Bao Xiaohua (鲍晓华), male, was born in 1972, professor, his main research interests are in the field of motor design, magnetic field analysis, and finite element analysis.

Abstract: Magnetic field generated by the pulse-current flowing into air-core reactor of the experimental advanced superconducting Tokamak (EAST) fast control power supply may cause a thermal problem in output cabinet. To solve the thermal problem, a layer or two layers of shielding are arranged around the air core reactor. When the maximum amplitude of the pulse current is 1 500A, the calculation method of magnetic field distribution around the air-core reactor is studied, as well as the output cabinet of eddy current loss. Taking eddy current loss as a main thermal source, three dimensional (3D) magnetic-thermal coupled finite element models of the reactor are established according to electromagnetism and thermodynamics theories. Temperature field of air-core reactor is analyzed and discussed in this paper. The results show that the magnetic field around air-core reactor and the temperature of output cabinet are decreased under shielded condition.

Keywords: EAST fast control power supply, output cabinet, air-core reactor, magnetic field, shield, eddy current loss, temperature

EAST快控电源中空心电抗器磁热耦合分析

胡云鹏[1] 鲍晓华[1] 张 程[1] 陈远洋[1] 高 格[2]

（1. 合肥工业大学电气工程与自动化工程学院 合肥 23009
2. 中国科学院等离子体物理研究所 合肥 23000）

摘要：当脉冲电流通过实验先进超导托卡马克 (EAST) 快控电源中空心电抗器时会产生磁场，导致输出柜发热。为了解决热问题，在空心电抗器周围安装一层或两层屏蔽体。电流幅值最大为 1 500A 时，求解空心电抗器周围磁场分布以及输出柜的涡流损耗。将涡流损耗作为主要的热源，根据电磁学和热力学理论建立电抗器的三维磁热耦合有限元模型。本文对空心电抗器的温度场进行分析和讨论。结果表明，在屏蔽条件下空心电抗器的磁场和输出柜的温度都会降低。

关键词：EAST 快控电源 输出柜 空心电抗器 磁场 屏蔽体 涡流损耗温度

Project supported by the National Natural Science Funds of China (51377039, 51677051).

1 Introduction

Experimental advanced superconducting Tokamak (EAST) fast control power supply is a large capacity single phase inverter power supply[1]. The system consists of six H-bridges branches, and each branch has an air-core reactor. In this system, the reactor is employed to limit current, steady voltage and compensate reactive power. Recently, the analytical method has been used to calculate and analyze the magnetic field distribution in air-core reactor without shield[2-3]. Electromagnetic shielding is a technique that reduces or prevents coupling of undesired radiated electromagnetic energy into equipment, so as to keep its operating compatibly with its electromagnetic environment. In order to shield the magnetic field, many scholars study a wide variety of shields, shields of different shapes and the number of layers[4-6]. In practical applications, air-core reactor during operation is prone to faults, including partial discharge, overheating and burnout[7-8]. The temperature rise is one of the main aging mechanisms that have to be considered, especially for the overall system; therefore, installing a shield for reactor is attracting more and more attention[9-11].

With regard to shield design problems, optimization is usually minimization of the field in a predefined area – the target region – and minimization of electromagnetic losses in a shield. However, it is also useful to include thermal aspects: a shield may obtain a high temperature because of electromagnetic losses and heat radiation from the heat source[12-13]. Even if the average temperature rise satisfies design requirement, the hottest-spot temperature in reactor might exceed the maximum temperature limits of insulation materials. Moreover, thermal field was simulated by finite-element method (FEM) after calculating the heat transfer coefficient by using nusselt number[14-15]. In calculation, the fluid dynamic behavior cannot be accurately described without using simulating fluid field. The calculation results were very different from the measurement results, so the heat transfer coefficient must be repeatedly modified. Therefore, a coupled analysis of magnetic field and thermal field is mandatory to compute the temperature rise in the design stage.

The purpose of this paper is to present a magnetic-thermal coupled model to accurately and efficiently predict the temperature in output cabinet, and use special shield made of composite materials to absorb strong magnetic field generated by the reactor. Different shielding materials will bring different results. When single-shielded, the effect of DT4A is the best and the effect of DT4A/GO is the best in two layers of shield. Temperature in single and double shielded condition reduces 38.1% and 64.2%, respectively. Comparing the simulation and measurement temperature, it can be seen that the error is within the controllable range. Therefore, thermal problem of the cabinet can be solved in this way.

2 Formulation

2.1 Structure of air-core reaction

The air-core reactor is mainly used for power supply rectifier which is intended to resolve the problem of inconsistencies in parallel rectifying element pressure drop. The reactor is made of 32 turns of winding copper coils and each coil is encapsulated glass fibers impregnated with epoxy resin.

This structure enhances electric strength, insulation strength and mechanical strength of the air-core reactor. Simulation and actual models of the reactor are shown in Fig.1. Three reactors in the middle of the cabinet, the distance between the cabinet and the reactor is 240mm and the distance between the adjacent reactor distances is 330mm.

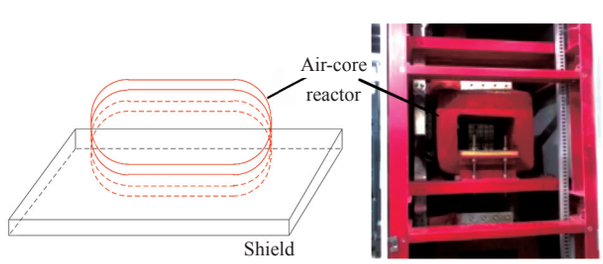

Fig.1 Models of the air-core reactor

2.2 Analytic calculation of magnetic field around air-core reactor

Fig.2 shows the irregular shape of each copper

coil, it is approximated as rectangular and composed of four elliptical arc edges. So the magnetic field of air-core reactor can be obtained by analyzing the magnetic field of each coil.

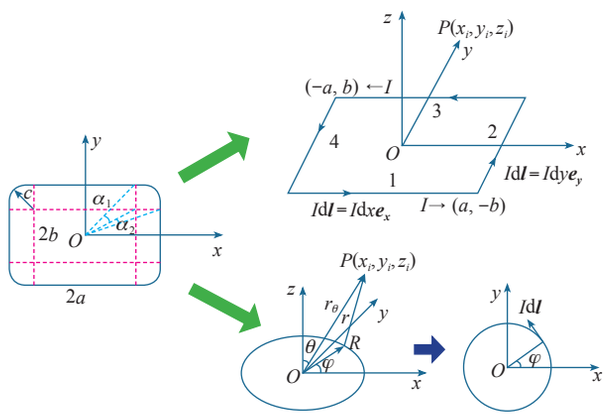

Fig.2 The model of single copper coil

For calculating magnetic field around air-core reactor, its motion equation is given by Biot-savart law. All parameters are shown in Fig.2.

$$\boldsymbol{B}=\frac{\mu_0}{4\pi}\int_l\frac{I\mathrm{d}\boldsymbol{l}}{r^2}\times\boldsymbol{e}_r \tag{1}$$

Where μ_0 denotes the permeability of free space, $I\mathrm{d}\boldsymbol{l}$ is current element.

(1) Magnetic field of rectangle line current. In this paper, the axis is the longitudinal direction of the magnet, and the current is defined as positive when it flows towards the positive x axis. It should be stated that for the rectangular winding the magnetic flux density will be composed from the shares of each of the rectangle side. It is assumed that the length $\mathrm{d}\boldsymbol{l}$ of the current element is infinite small. The unit vector between point $S(x, -b, z)$ on the wire 1 and arbitrary point $P(x_i, y_i, z_i)$ can be expressed as

$$\boldsymbol{e}_r=\frac{\boldsymbol{r}}{r}=\frac{(x_i-x)\boldsymbol{e}_x+(y_i+b)\boldsymbol{e}_y+(z_i-z)\boldsymbol{e}_z}{\sqrt{(x_i-x)^2+(y_i+b)^2+(z_i-z)^2}} \tag{2}$$

Where e_x、e_y and e_z denote the unit vector along the x、y and z axis.

According to Eq.(1) and Eq.(2), the induced magnetic field at arbitrary field point P is expressed as

$$\begin{aligned}\mathrm{d}B_1&=\frac{\mu_0}{4\pi}\frac{I\mathrm{d}x\boldsymbol{e}_x\times\boldsymbol{e}_r}{r^2}\\&=\frac{\mu_0 I\mathrm{d}x\boldsymbol{e}_x\times[(x_i-x)\boldsymbol{e}_x+(y_i+b)\boldsymbol{e}_y+(z_i-z)\boldsymbol{e}_z]}{4\pi[(x_i-x)^2+(y_i+b)^2+(z_i-z)^2]^{3/2}}\end{aligned} \tag{3}$$

So the x_i, y_i, z_i component of the magnetic flux density is

$$\begin{cases}\mathrm{d}B_{1x_i}=0\\ \mathrm{d}B_{1y_i}=-\dfrac{\mu_0 I(z_i-z)}{4\pi[(x_i-x)^2+(y_i+b)^2+(z_i-z)^2]^{3/2}}\mathrm{d}x\\ \mathrm{d}B_{1z_i}=\dfrac{\mu_0 I(y_i+b)}{4\pi[(x_i-x)^2+(y_i+b)^2+(z_i-z)^2]^{3/2}}\mathrm{d}x\end{cases} \tag{4}$$

The total magnetic field at point P generated by wire 1 is given as

$$\begin{cases}B_{1y_i}=-\int_{-a}^{a}\dfrac{\mu_0 I(z_i-z)}{4\pi[(x_i-x)^2+(y_i+b)^2+(z_i-z)^2]^{3/2}}\mathrm{d}x\\ \quad=\dfrac{\mu_0 I(z_i-z)}{4\pi[(y_i+b)^2+(z_i-z)^2]}\left[\dfrac{(x_i-a)}{r_1}-\dfrac{(x_i+a)}{r_2}\right]\\ B_{1z_i}=\int_{-a}^{a}\dfrac{\mu_0 I(y_i+b)}{4\pi[(x_i-x)^2+(y_i+b)^2+(z_i-z)^2]^{3/2}}\mathrm{d}x\\ \quad=\dfrac{\mu_0 I(y_i+b)}{4\pi[(y_i+b)^2+(z_i-z)^2]}\left[\dfrac{(q-x_i)}{r_1}+\dfrac{(a+x_i)}{r_2}\right]\end{cases} \tag{5}$$

With

$$\begin{cases}r_1=\sqrt{(x_i-a)^2+(y_i+b)^2+(z_i-z)^2}\\ r_2=\sqrt{(x_i+a)^2+(y_i+b)^2+(z_i-z)^2}\end{cases} \tag{6}$$

Similarly, magnetic field at point P generated by wire 2、3 and 4 can also be calculated. So the magnetic field of rectangle line current is

$$\begin{cases}B_{rx_i}=\dfrac{\mu_0 I(z_i-z)}{4\pi[(x_i-a)^2+(z_i-z)^2]}\left[\dfrac{(b-y_i)}{r_3}+\dfrac{(b+y_i)}{r_1}\right]+\\ \quad\dfrac{\mu_0 I(z_i-z)}{4\pi[(x_i+a)^2+(z_i-z)^2]}\left[\dfrac{(y_i-b)}{r_4}-\dfrac{(b+y_i)}{r_2}\right]\\ B_{ry_i}=\dfrac{\mu_0 I(z_i-z)}{4\pi[(y_i+b)^2+(z_i-z)^2]}\left[\dfrac{(x_i-a)}{r_1}-\dfrac{(x_i+a)}{r_2}\right]+\\ \quad\dfrac{\mu_0 I(z_i-z)}{4\pi[(y_i-b)^2+(z_i-z)^2]}\left[\dfrac{(a-x_i)}{r_3}+\dfrac{(x_i+a)}{r_4}\right]\\ B_{rz_i}=\dfrac{\mu_0 I(y_i+b)}{4\pi[(y_i-b)^2+(z_i-z)^2]}\left[\dfrac{(a-x_i)}{r_1}+\dfrac{(a+x_i)}{r_2}\right]+\\ \quad\dfrac{\mu_0 I(y_i-b)}{4\pi[(y_i-b)^2+(z_i-z)^2]}\left[\dfrac{(x_i-a)}{r_3}-\dfrac{(a+x_i)}{r_4}\right]+\\ \quad\dfrac{\mu_0 I(x_i-a)}{4\pi[(x_i-a)^2+(z_i-z)^2]}\left[\dfrac{(y_i-b)}{r_3}-\dfrac{(y_i+b)}{r_1}\right]+\\ \quad\dfrac{\mu_0 I(x_i+a)}{4\pi[(x_i+a)^2+(z_i-z)^2]}\left[\dfrac{(b-y_i)}{r_4}+\dfrac{(y_i+b)}{r_2}\right]\end{cases} \tag{7}$$

With

$$\begin{cases} r_3 = \sqrt{(x_i - a)^2 + (y_i - b)^2 + (z_i - z)^2} \\ r_4 = \sqrt{(x_i + a)^2 + (y_i - b)^2 + (z_i - z)^2} \end{cases} \tag{8}$$

(2) Magnetic field of oval line current. Fig.2 shows an oval current-carrying coil, and the oval equation is

$$\frac{x^2}{(a+c)^2} + \frac{y^2}{b^2} = 1 \tag{9}$$

Through the transformation, solving the magnetic field distribution of elliptical coils can be converted into solving circular coil magnetic field distribution. Assuming elliptical shape factor $k = b/a$ and $X = k^{1/2}x$, $Y = k^{-1/2}y$, Eq.(9) becomes

$$X^2 + Y^2 = (a+c)b \tag{10}$$

With

$$R = (a+c)b \tag{11}$$

Some equations can be obtained by Fig.2.

$$\begin{cases} \boldsymbol{r}_\theta = r_\theta(\sin\theta \boldsymbol{e}_x + \cos\theta \boldsymbol{e}_z) \\ R = \boldsymbol{R}(\cos\varphi \boldsymbol{e}_x + \sin\varphi \boldsymbol{e}_y) \\ r^2 = r_\theta^2 + R^2 - 2r_\theta \sin\theta\cos\varphi \\ \mathrm{d}\boldsymbol{l} = R(-\sin\varphi \boldsymbol{e}_x + \cos\varphi \boldsymbol{e}_y)\mathrm{d}\varphi \end{cases} \tag{12}$$

In actual space, the magnetic flux density of any point can be obtained by the series of limited items. According to Eq.(1)、Eq.(12) and complete elliptic integrals, the magnetic field of oval line current is given as

$$\begin{cases} B_{ox_i} = \dfrac{\mu_0 I R r_\theta \cos\theta}{2(r_\theta^2 + R^2)^{3/2}} \displaystyle\sum_{n=1}^{\infty} C_n \left(\frac{2Rr_\theta \sin\theta}{r_\theta^2 + R^2} \right)^{2n-1} \\ B_{oz_i} = \dfrac{\mu_0 I R^2}{2(r_\theta^2 + R^2)^{3/2}} + \dfrac{\mu_0 I R^2}{2(r_\theta^2 + R^2)^{3/2}} \displaystyle\sum_{n=1}^{\infty} D_n \left(\frac{2Rr_\theta \sin\theta}{r_\theta^2 + R^2} \right)^{2n} - \\ \qquad \dfrac{\mu_0 I R r_\theta \cos\theta}{2(r_\theta^2 + R^2)^{3/2}} \displaystyle\sum_{n=1}^{\infty} C_n \left(\frac{2Rr_\theta \sin\theta}{r_\theta^2 + R^2} \right)^{2n-1} \end{cases} \tag{13}$$

With

$$\begin{cases} r_\theta = \sqrt{x_i^2 + (z_i - z)^2} \\ C_n = \dfrac{1}{(2n-1)!} \dfrac{(4n-1)(4n-3)\cdots 3}{2^{(2n-1)}} \dfrac{(2n-1)(2n-3)\cdots 1}{2n(2n-2)\cdots 2} \quad n \in N \\ D_n = \dfrac{1}{2n} \dfrac{(4n+1)(4n-1)\cdots 3}{2^{2n}} \dfrac{(2n-1)(2n-3)\cdots 1}{2n(2n-2)\cdots 2} \quad n \in N \end{cases} \tag{14}$$

With the analysis above, magnetic field around air-core reactor is

$$B = \sum_{i=1}^{32} \sqrt{\left[\frac{2(\alpha_1 + \alpha_2)}{\pi} B_{ox_i} + B_{rx_i} \right]^2 + B_{ry_i}^2 + \left[\frac{2(\alpha_1 + \alpha_2)}{\pi} B_{oz_i} + B_{rz_i} \right]^2} \tag{15}$$

With

$$\begin{cases} \alpha_1 = \arccos \dfrac{a^2 + b^2 - bc}{\sqrt{a^2 + b^2}\sqrt{a^2 + (b-c)^2}} \\ \alpha_2 = \arccos \dfrac{a^2 + (a+c)^2 + 2(b-c)^2 - c^2}{2\sqrt{a^2 + (b-c)^2}\sqrt{(a+c)^2 + (b-c)^2}} \end{cases} \tag{16}$$

Where B_{ox_i}、B_{oz_i} is magnetic flux density in the direction of each axis of elliptical coil, B_{rx_i}、B_{ry_i} and B_{rz_i} is magnetic flux density representing the direction of the rectangular coil.

For Eq.(15), the flux density at any point in actual space can be approximated by the series of limited entry and the magnetic flux density distribution of output cabinet can be calculated. So the eddy current loss in output cabinet can be analyzed by electromagnetic induction law and Ohms law. The equation is expressed as

$$P_e = \frac{\pi^2}{6\rho}(fB)^2 \Delta_{Fe}^3 lh \tag{17}$$

Where Δ_{Fe}、h、and l are thickness、height and length of the output cabinet respectively, ρ is iron conductivity.

(3) Strong coupling of magnetic-thermal field calculation. Fig.3 illustrates the Joule heat taken away from output cabinet by the cooling modes including

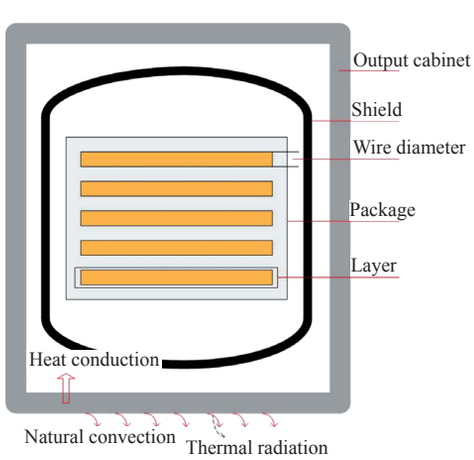

Fig.3 Axisymmetric model of air-core reactor

heat conduction, natural convection and thermal radiation. The air-core reactor consists of 32-layers copper coils, some of which are shown in Fig.3. From the quantitative analysis point of view, it is necessary to establish a mathematical model in which the magnetic field equations, the heat conduction equation and the Navier-Stokes equations are linked through coupled variables.

For the system of the reactor shown in Fig.3, there are three heat dissipation modes, involving heat conduction, natural convection and thermal radiation. For the output cabinet, the main heat dissipation mode is heat conduction. For the surface between output cabinet and surrounding air, the main heat dissipation mode is natural convection and thermal radiation. Finally, the temperature distributions of the output cabinet should be concerned.

1) Heat conduction. For the output cabinet, the steady state heat conduction equation for solid is given as

$$\frac{\partial}{\partial x}\left(\lambda\frac{\partial T}{\partial x}\right)+\frac{\partial}{\partial y}\left(\lambda\frac{\partial T}{\partial y}\right)+\frac{\partial}{\partial z}\left(\lambda\frac{\partial T}{\partial z}\right)+Q=0 \tag{18}$$

Where λ is the coefficient of heat conductivity, Q is the heat generation of unit volume in iron conductors

2) Natural convection. The natural convection of air satisfies the Navier-Stokes equations, which consist of three groups of equations. For three dimensional incompressible steady fluids, the Navier-Stokes equations in Cartesian coordinate system can be simplified as following

Continuity equation

$$\frac{\partial(\rho u)}{\partial x}+\frac{\partial(\rho v)}{\partial y}+\frac{\partial(\rho w)}{\partial z}=0 \tag{19}$$

Momentum conservation equations

$$\begin{cases}\rho u\dfrac{\partial u}{\partial x}+\rho v\dfrac{\partial u}{\partial y}+\rho w\dfrac{\partial u}{\partial z}=\mu\nabla^2 u-\dfrac{\partial P}{\partial x}+f_x\\ \rho u\dfrac{\partial v}{\partial x}+\rho v\dfrac{\partial v}{\partial y}+\rho w\dfrac{\partial v}{\partial z}=\mu\nabla^2 v-\dfrac{\partial P}{\partial y}+f_y\\ \rho u\dfrac{\partial w}{\partial x}+\rho v\dfrac{\partial w}{\partial y}+\rho w\dfrac{\partial w}{\partial z}=\mu\nabla^2 w-\dfrac{\partial P}{\partial z}+f_z\end{cases} \tag{20}$$

Energy equation is given as

$$\rho c\left(u\frac{\partial T}{\partial x}+v\frac{\partial T}{\partial y}+w\frac{\partial T}{\partial z}\right)=\lambda\nabla^2 T+Q \tag{21}$$

Where ρ is fluid density, μ is viscosity coefficient, c is the specific heat, u、v and w are the respective x、y and z direction potentials of the fluid speed, P is the fluid pressure, T is the fluid temperature, f_x、f_y and f_z are the sources in the respective x、y and z directions.

3) Thermal radiation. For a system of two surfaces (surface i and j) radiating to each other, the heat transfer rate between surfaces i and j is expressed as

$$Q_{ij}=\sigma\varepsilon_i\beta_{ij}A_i(T_i^4-T_j^4) \tag{22}$$

Where σ is Stefan-Boltzmann constant, ε_i is the effective emissivity of surface i, β_{ij} represents the radiation view factor between surface i and j, A_i is the area of surface i, and T_i、T_j represent the absolute temperature of surface i and j.

3 Calculations of a air-core reactor

(1) Analysis of shielding thickness. To limit the leakage magnetic field inside the shield and use materials efficiently, the thickness of the shield should be considered. Penetration depth of the shield is expressed as

$$\delta=\sqrt{\frac{1}{\pi f\mu\sigma}} \tag{23}$$

Where μ is permeability of conductor, σ is conductivity of conductor.

Take a reference line through the shield, it can be seen that the depth of the shield is based on the magnetic density of the reference line. Where the magnetic flux is high, the magnetic field passes. This distance is the penetration depth of high magnetic flux. Fig.4 shows penetration depth and magnetic flux density of the shield when AC amplitude and

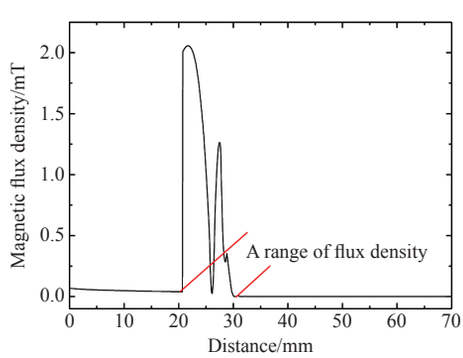

Fig.4 Penetration depth of the shield

frequency are 1 500A and 100Hz, respectively. Obviously, the penetration depth of the magnetic field shield does not exceed 20mm. Eq.(23) shows that penetration depth increases as the frequency decreases. To ensure that the magnetic field does not penetrate the shield, thus thickness of the shield is selected as 20mm.

A shield is a metallic partition placed between two regions of space. It is used to control the propagation of electromagnetic fields from one region to the other. Shield changes not only the size of the magnetic flux density but also the direction of the magnetic field. Fig.5a shows the magnetic flux density distribution in no-shielded condition. It can be seen that the magnetic field around the four corners of the reactor is the strongest, and the center is the weakest. Because magnetic line is a loop formed from the inside to the outside. The magnetic flux densities around output cabinet in single shielded and double shielded condition are shown in Fig.5b and Fig.5c, respectively. Obviously, magnetic flux density is reduced in shielded condition and this phenomenon is more obvious when the double layer metal plate shields. When using the double shielding metal plate

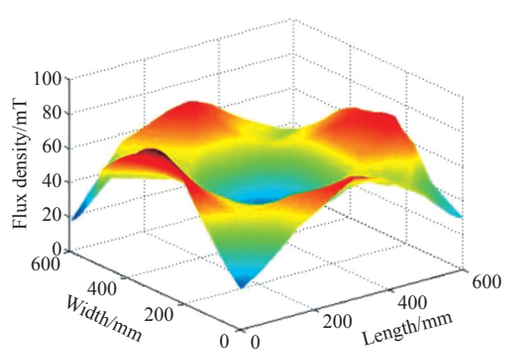

(a) Distribution of magnetic flux density in no-shielded condition

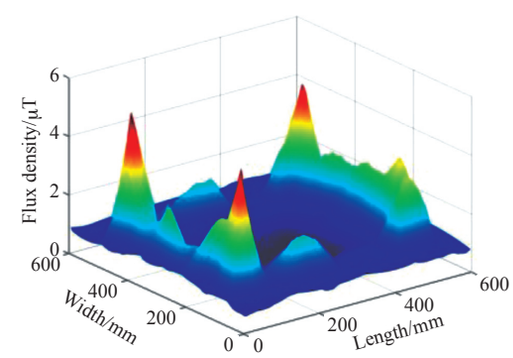

(b) Distribution of magnetic flux density in single shielded (DT4A) condition

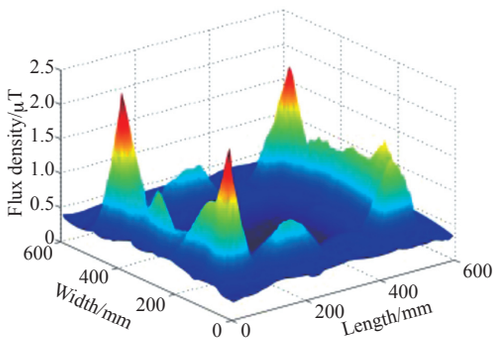

(c) Distribution of magnetic flux density in double shielded (DT4A/GO) condition

Fig.5 The magnetic flux density distribution

(DT4A/GO, DT4A is closer to the field source), the shielding effect is better.

(2) The influence of shield. Fig.6 represents the schematic drawing of simulation setup for simulating an air-core reactor shielding system. The reactor is surrounded by a shield, and the shield is between the reactor and output cabinet. The reference point is taken from the coordinate origin and multiple sets of data can be obtained from the reference point to judge the performance of shield.

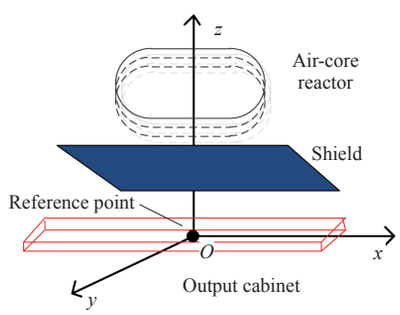

Fig.6 Schematic drawing of the simulation setup

The shield can be in any position between the reactor and output cabinet. So, the distance between shield and reference point can be changed.

Magnetic field was measured from the reference point on the output cabinet. Fig.1 shows the linear relation between cabinet and the resultant magnetic field with shields. The shielding materials were grain-oriented electrical steel (GO), electrical pure iron (DT4A) and 1008 steel. All the materials are 20mm thick, and take amplitude (1 500A) of current which flow through air-core reactor. As a surrogate of shielding performance, shielding factor (SF) is used.

It is defined as the ratio of shielded magnetic field to unshielded magnetic field as follows

$$SF = 20\lg\left|\frac{B_{unshielded}}{B_{shielded}}\right| \quad (24)$$

The greater the value of SF, the better the shielding effect.

For magnetic fields generated by the reactor, the variation of the shielding factor as a function of distance is shown in Fig.7a. The reference point is fixed, and the metal plate moves toward the z axis at every 20mm distance. A noticeable reduction of magnetic fields by the shields is observed when the current (1 500A, 30kHz) flows through the reactor. When installing GO, matching the direction of grain orientation with field direction is important. Longitudinal direction of the GO sheets is an easy magnetization direction, whereas DT4A and 1008 steel are magnetically isotropic. In the case of single layer shielding, single layer shielding factor (SF_1) of the three magnetic materials decreases with increasing distance. In the three materials, shielding effect of DT4A is the best and the maximum SF_1 is 105dB. Whereas, the shielding effect of 1008 steel is the best and the maximum SF_1 is 54.3dB. Shielding factor of DT4A compared with 1008 steel is higher than 48.2%. Taking into account all aspects, DT4A shows the most effective shielding performance at the electric current. Fig.7b shows the relationship between SF_2 (double layer shielding factor) and distance. When distance between the double layer shield and the reference point is not the same, the size of SF_2 will be changed. The distance from the reference point of shield can be moved as needed, as shown in Fig.7b. SF_2 is inversely proportional to the distance, the smaller the distance, the greater the SF_2. Although the six kinds of results are similar, but the shielding effect of DT4A/GO (DT4A is closer to the field source) is better. Therefore DT4A/GO as a shielding material is more appropriate.

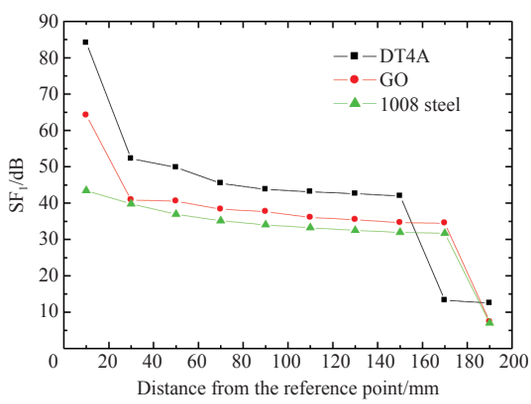

(a) Relationship between SF_1 and distance

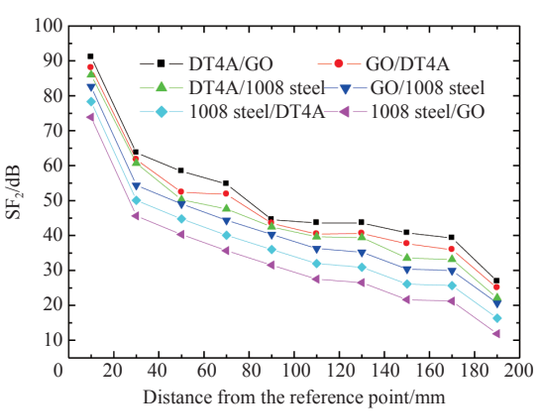

(b) Relationship between SF_2 and distance

Fig.7 Relationship between SF_1、SF_2 and distance

EAST fast control power provides a current and the range of current frequency is 100Hz to 30 kHz. Fig.8a and Fig.8b show single and double layer shielding factor of different frequency respectively. In this case, it can be seen that no matter what kind of combination, with the increase in frequency, SF_1 and SF_2 are gradually increased. Among these groups, DT4A/GO has the best shielding effect. Maximum shielding factor can be reached 121.45dB. 1008 steel of the performance is the worst and the maximum shielding factor is 72dB. With the change of frequency, the double layer shielding method is more effective for shielding electromagnetic field.

This result demonstrates that closely adjacent layers act as one body under the regime of shunt mechanism of magnetic shielding. For example, SF of closely adjacent DT4A/GO is simply dependent on an averaged permeability of DT4A and GO. On the other hand, the DT4A effectively reduces the strong magnetic field first, and then the GO sheet effectively shields the weakened field. In the case of 1008 steel/GO pair, shielding performance was not improved since a strong magnetic field near the source was too high to be effectively shielded by 1008 steel. From the above analysis, it can be concluded that DT4A is

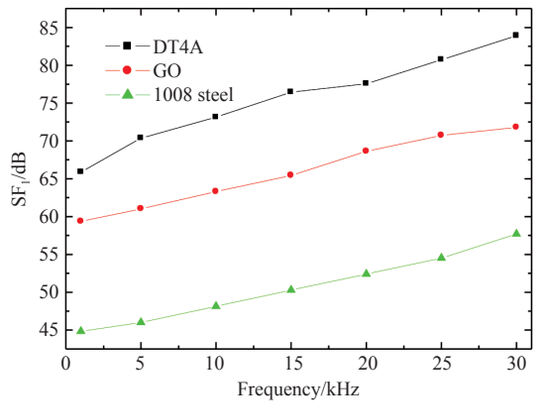

(a) Single layer shielding factor of different frequency

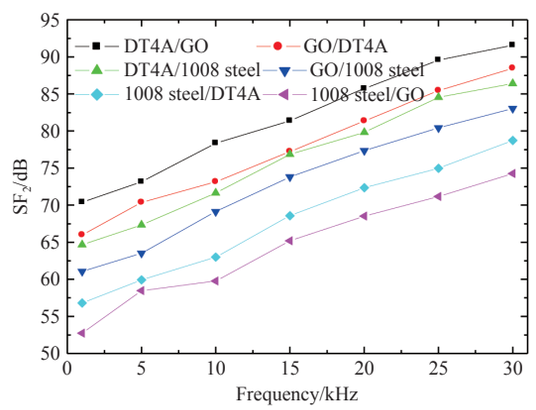

(b) Double layer shielding factor of different frequency

Fig.8 Single and double layer shielding factor of different frequency

the best one in terms of distance factor and frequency factor.

(3) The temperature and eddy current loss of output cabinet. The temperature and eddy current loss of output cabinet can be simulated by ANSOFT and ANSYS Workbench. First, the eddy current density of the cabinet can be calculated. Then, the results will be imported into ANSYS Workbench. Finally, temperature distribution can be obtained by the two software and adding material. In no-shielded condition, the eddy current loss and temperature are 1 225.2W and 68.5℃. Tab. shows the eddy current loss and temperature of the output cabinet under different shielding materials when pulse current flowing into air-core reactor. It can be seen that temperature in shielded condition reduces by 64.2% of no-shielded condition.

The temperatures of the cabinet in shielded (DT4A/GO) and no-shielded condition are compared in Fig.9a and Fig.9b. As can be seen from the

Tab. The eddy current loss and temperature of the output cabinet under different shielding materials

Material	Eddy current loss/W	Temperature/℃
GO	922.9	51.6
DT4A	758.4	42.4
1008 steel	1 087.5	60.8
DT4A/GO	438.2	24.5
GO/DT4A	499.0	27.9
DT4A/1008 steel	550.9	30.8
1008 steel/ DT4A	613.5	34.3
GO/1008 steel	581.3	32.5
1008 steel/GO	620.6	37.6

temperature distribution diagram, the four sides of the temperature are relatively high, and this is exactly the case with the distribution of flux density. Simulation of the temperature in no-shielded condition and shielded condition error are 4.5% and 2.2%. Comparing the measured and simulated data, it can be seen that the thermal problem can be effectively solved by using shield to absorb strong magnetic field.

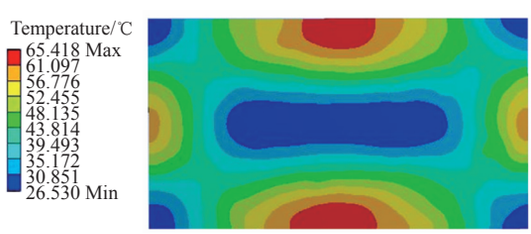

(a) Distribution of temperature in no-shielded condition

(b) Distribution of temperature in shielded (DT4A/GO) condition

Fig.9 Distribution of temperature in no-shielded and shielded condition

5 Conclusion

In this paper the magnetic field and thermal field by experiment and FEM are analyzed. Magnetic shielding performances of three shielding materials in the vicinity of a center line on the output cabinet have been evaluated. In shielding with a single layer,

DT4A shows the best shielding performance. DT4A/GO is the most effective shield in shielding with two layers. In sum, the minimum temperature of the cabinet dropped to 24.5℃ by this measure. Finally, the thermal problem is effectively solved.

References

[1] Huang Haihong, Wang Haixin, Gao Ge, et al. Application of phase-shift PWM in EAST fast control power supply[J]. IEEE Transactions on Applied Superconductivity, 2010, 20(3): 1671-1675.

[2] Yu Qin, Sebo S A. Calculation accuracy of the planar filament current loop stack model of large air-core reactor coils[J]. IEEE Transactions on Magnetics, 1997, 33(5): 3313-3315.

[3] Yu Qin, Sebo S A. Accurate evaluation of the magnetic field strength of large substation air-core reactor coils[J]. IEEE Transactions on Power Delivery, 1998, 13(4): 1114-1119.

[4] Su Y P, Liu Xun, Hui S Y R. Mutual inductance calculation of movable planar coils on parallel surfaces[J]. IEEE Transactions on Power Electronics, 2009, 24(4): 1115-1123.

[5] Moser J R. Low-frequency low-impedance electromagnetic shielding[J]. IEEE Transactions on Electromagnetic Compatibility, 1988, 30(3): 202-210.

[6] Oktem M H, Saka B. Design of multilayered cylindrical shields using a genetic algorithm[J]. IEEE Transactions on Electromagnetic Compatibility, 2001, 43(2): 170-176.

[7] Sergeant P, Adriano U, Dupre L, et al. Active and passive magnetic shielding for stray field reduction of an induction heater with axial flux[J]. IEEE Transactions on Magnetics, 2004, 40(2): 675-678.

[8] Liu Z G, Geng Y S, Wang J H, et al. Design and analysis of new type air-core reactor based on coupled fluid-thermal field calculation[J]. Transactions of China Electrotechnical Society, 2003, 18(6): 59-63.

[9] Sergeant P, Dupre L, Melkebeek J. Active and passive magnetic shielding for stray fieldreduction of an induction heater with axial flux[J]. IEE Proceedings-Electric Power Applications, 2005, 152(5): 1359-1364.

[10] Yoshizawa K, Noguchi S, Igarashi H. Influence of magnetic property of ferromagnetic shield on high field magnet analysis[J]. IEEE Transactions on Applied Superconductivity, 2011, 21(3): 2088-2091.

[11] Bavastro D, Canova A, Giaccone L. Numerical and experimental development of multilayer magnetic shields[J]. Electric Power Systems Research, 2014, 116(11): 374-380.

[12] Sergeant P, Hectors D, Dupre L, et al. Thermal analysis of magnetic shields for induction heating[J]. IET Electric Power Applications, 2009, 3(6): 543-550.

[13] Ho S L, Li Y, Lin X, et al. A 3-D study of eddy current field and temperature rises in a compact bus duct system[J]. IEEE Transactions on magnetics, 2006, 42(4): 987-990.

[14] Ranran Lin, Haavisto A, Arkkio A. Analysis of eddy-current loss in end shield and frame of a large induction machine[J]. IEEE Transactions on Magnetics, 2010, 46(3): 942-948.

[15] Ho S L, Li Y, Lin X, et al. Calculations of eddy current, fluid, and thermal fields in an air insulated bus duct system[J]. IEEE Transactions on Magnetics, 2007, 43(4): 1433-1436.